Inorganic Chemistry

Article

pubs.acs.org/IC

# Kinetic Aspects for the Reduction of $CO_2$ and $CS_2$ with Mixed-Ligand Ruthenium(II) Hydride Complexes Containing Phosphine and Bipyridine

Jing Huang,[†] Jinzhu Chen,*[,†] Hui Gao,[†,‡] and Limin Chen[‡]

[†]CAS Key Laboratory of Renewable Energy, Guangzhou Institute of Energy Conversion, Chinese Academy of Sciences, Guangzhou 510640, P. R. China

[‡]Guangdong Provincial Key Laboratory of Atmospheric Environment and Pollution Control, College of Environment and Energy, South China University of Technology, Guangzhou 510006, P. R. China

Supporting Information

**ABSTRACT:** A new water-soluble ruthenium hydride complex $[Ru(H)(bpy)_2(PTA)]PF_6$ (bpy = 2,2′-bipyridine, PTA = 1,3,5-triaza-7-phosphaadamantane) (**1a**) was prepared. **1a** reacted with $CO_2$ and $CS_2$ to give the corresponding formate and dithioformate complexes, respectively. Both the insertions of $CO_2$ and $CS_2$ into the Ru−H bond of **1a** followed second-order kinetics. The second-order rate constant ($k_2$) of $CO_2$ insertion reaction varied from $(9.40 \pm 0.41) \times 10^{-4}$ $M^{-1}$ $s^{-1}$ in acetone to $(1.13 \pm 0.08) \times 10^{-1}$ $M^{-1}$ $s^{-1}$ in methanol; moreover, the $\ln(k_2)$ is in good linear relationship with the acceptor number (AN) of the solvent used. Although, the $k_2$ of $CS_2$ insertion reaction ranged from $(3.43 \pm 0.10)$ $M^{-1}$ $s^{-1}$ in methanol to $(24.0 \pm 0.5)$ $M^{-1}$ $s^{-1}$ in *N*,*N*-dimethylformamide, which is 1000 times faster than $CO_2$ insertion. Generally, the $k_2$ of $CS_2$ insertion increased with the static dielectric constant ($D_s$) of the reaction medium investigated. For comparison purposes, we further investigated the reactivity of $[Ru(H)(bpy)_2(PPh_3)]PF_6$ ($PPh_3$ = triphenylphosphine) (**1b**) with $CO_2$ and $CS_2$. **1b** reacted with $CO_2$ slowly in the methanol with a $k_2$ of $(1.46 \pm 0.09) \times 10^{-3}$ $M^{-1}$ $s^{-1}$, yielding a formate complex $[Ru(\eta^1\text{-}OC(H)=O)(bpy)_2(PPh_3)]PF_6$ (**2b**). The reaction of **1b** with $CS_2$ is 1000 times faster than that of $CO_2$. The structures of **1a**, **1b**, and **2b** were determined by X-ray crystallographic analysis.

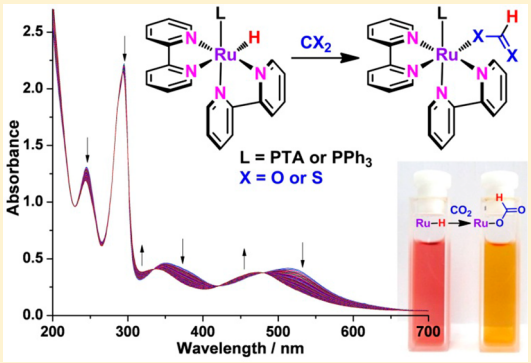


## INTRODUCTION

Reduction of carbon dioxide ($CO_2$) to liquid fuels, organic chemicals, and carbohydrates has attracted much attention in the past few decades, owing to the fact that $CO_2$ is recognized as a safe, economical, and renewable carbon source.[1−8] The reduction method for $CO_2$ involves photocatalysis, electrocatalysis, and hydrogenation. In the research field of photochemical $CO_2$ reduction, sunlight is generally used as the energy source to produce CO and formate by the coupling of light absorption and charge separation with a dark reaction.[1,2] In the case of electrochemical reduction of $CO_2$, productions of hydrocarbons, alcohols, formate, and CO are generally obtained with electrocatalysts as electron transfer agents and electrical potential as the driving force.[3,4,9] In addition to sunlight and electrical potential, a molecular hydrogen ($H_2$) is another important energy to convert $CO_2$ into fuels and organic chemicals through $CO_2$ hydrogenation reaction, which includes homogeneous hydrogenation with molecular catalysis and a reverse water−gas shift reaction (RWGS reaction).[5−8,10] In the $CO_2$ hydrogenation, the step of $CO_2$ insertion into the metal hydride bond of a metal hydride species leads to a metal formate complex, which is crucial to the $CO_2$ reduction and the catalysis.[11−23] These metal hydride complexes were also suggested as important "intermediates" and truly "active species" for homogeneous hydrogenation of the $CO_2$.[6−8,24−27] In addition, the highly reducing nature of these metal hydride complexes makes them potential mediators in the solar generation of fuels and electrochemical formation of chemicals.[1,3] Accordingly, the reduction of $CO_2$, catalyzed by metal hydride complexes or with metal hydride complexes as "intermediates," has been intensively studied in experiments[28−33] and theory[34−40] to explore the mechanism.[41−44] Currently, the metal hydride complexes are of particular interest for mechanism and kinetics studies for $CO_2$ reduction due to their hydride-donating power and reducing nature.

In the literature of mechanism and kinetics research for $CO_2$ reduction with metal hydride complexes, Ishitani and coworkers reported the reactions of $[Ru(H)(tpy)(4,4\text{-}X_2bpy)]^+$ (tpy = 2,2′:6′,2″-terpyridine, bpy = 2,2′-bipyridine, X = H and OMe) and $CO_2$ in various solvents.[17] They found that the Lewis-acid character of solvent affects the fixation process. Moreover, the authors further suggested that the nucleophilic attack of the hydride ligand to the carbon atom of $CO_2$ is the

Received: April 14, 2014
Published: August 28, 2014

   dx.doi.org/10.1021/ic500866d | Inorg. Chem. 2014, 53, 9570−9580

rate-determining step in the $CO_2$ insertion reaction. Matsubara and Hirao theoretically explored the mechanism of hydrido migration from metal hydride complexes to $CO_2$ and indicated that the reactivity of metal hydride complexes depends on the metal, solvent, and substrate.[33] Moreover, the favorable path for hydrido migration can mutually be switched by the above effects. Fujita and co-workers recently reported a rhenium complex *fac*-ReCl($\alpha$-diimine)$(CO)_3$ containing an $NAD^+$ model ligand. They examined its reactivity toward photochemical formation of the corresponding NADH-like dihydro form of the complex and electrochemical $CO_2$ reduction.[44] Muckerman and co-workers provided a deeper insight into a correlation between experimental and density functional theory-derived results of the hydride-donating power of various metal and organic hydride donors.[34] Lau and co-workers prepared a series of novel ruthenium hydride complexes with the intramolecular N−H···H−Ru proton−hydride interaction, $[(\eta^5\text{-}C_5H_4(CH_2)_nNMe_2H^+)Ru(H)(dppm)]$ [$n$ = 2, 3; dppm = 1,1-bis(diphenylphosphino)methane]. By using these ruthenium hydride complexes as catalysts, they further systematically investigated the hydrogenation of $CO_2$ to formic acid in tetrahydrofuran.[30] The proposed mechanism involves $CO_2$ insertion into the Ru−H bond of the ruthenium hydride complexes followed by the protonation of a formato ligand by a intramolecular N−H group. Nozaki and co-workers reported hydrogenation of $CO_2$ with pincer Ir(III) hydride complexes as catalysts, in which an equilibrium between trihydridoiridium(III) complex and dihydridoiridium(III) formate complex was observed upon exposure of the trihydride complex into 1 atm $CO_2$.[27]

In addition to the reactions between noble metal hydrides with $CO_2$, the migratory insertions of $CO_2$ into the Ni−H bonds of nickel hydride complexes to give nickel formate complexes were investigated by Guan et al., Hazari et al., Lee et al., and Tonzetich et al.[19−22] Field and co-workers investigated the insertion reactions of $CO_2$ into iron(II) hydride complexes such as *cis*-Fe(dmpe)$_2H_2$ (dmpe = $Me_2PCH_2CH_2PMe_2$) and *cis*-Fe$(PP_3)H_2$ ($PP_3$ = $P(CH_2CH_2PMe_2)_3$).[23] Recently, we compared the reactivity of iron(II) hydride complexes with that of their ruthenium analogues in $CO_2$ reduction.[14] It was found that the one-electron-reduction products of $[Ru(H)(bpy)(P(OEt)_3)_3]^+$ [$P(OEt)_3$ = triethyl phosphate] and $[Ru(H)(bpy)_2(P(OEt)_3)]^+$ and the two-electron-reduction product of $[Fe(H)(bpy)(P(OEt)_3)_3]^+$ react with $CO_2$ in acetonitrile.

In addition to organic solvent for $CO_2$ reduction, water is a desirable solvent and recognized to promote the reactions between $CO_2$ and metal hydride complexes.[12,16,31,32,36,38] Creutz and co-workers studied kinetics and the mechanism of hydride ion transfer from ruthenium complexes to $CO_2$ in water.[11−13] They suggested that the thermodynamics of formation of the hydride ion are responsible for the promoted hydride-transfer rate in water. By using a water-soluble ruthenium hydride complex $[(\eta^6\text{-}C_6Me_6)Ru(H)(bpy)](CF_3SO_3)$, Ogo and co-workers observed an accelerating effect of a proton on the reduction of $CO_2$ in aqueous media under acidic conditions.[16] Sakaki and co-workers studied the promotion effect of water molecules in ruthenium complex-catalyzed hydrogenation of $CO_2$. They suggested that the aqua ligand accelerates the nucleophilic attack of the H ligand to $CO_2$.[38] Moreover, a series of water-soluble metal hydride complexes such as $[(\eta^6\text{-}C_6Me_6)Ru(H)(4,4\text{-}X_2bpy)]^+$ and $[Cp^*Ir(H)(4,4\text{-}X_2bpy)]^+$ (X = H and OMe, Cp* = 1,2,3,4,5-pentamethylcyclopentadienyl), which are *in situ* generated from the hydrogenation of the corresponding aqua complexes, were suggested as important intermediates for aqueous hydrogenation of $CO_2$ to formate.[24,25]

Apart from $CO_2$, carbon disulfide ($CS_2$) is also an important carbon source.[45] Moreover, $CS_2$ is usually used as a model for $CO_2$ and carbonyl sulfide (COS) because $CS_2$ is more reactive and often displays similar binding modes.[46−54] For example, the migration of the hydrido ligand to $CS_2$ from ruthenium hydride complexes and iron hydride complexes similarly takes place in the experiment to give dithioformate complexes.[23,30] However, the coordination modes of formato and dithioformato ligands in transition metal complexes are usually different. The formato normally acts as an $\eta^1$-ligand in complexes[17] whereas dithioformato can function as an $\eta^1$- or $\eta^2$-ligand depending on the coordination environment of the central metals.[55,56] Matsubara et al. compared the insertion mechanism of $CS_2$ with $CO_2$ into a Ru−H bond in ruthenium hydride complexes. They suggested that the difference between the reaction of $CS_2$ and $CO_2$ with metal hydride complexes is attributed to the different charge distribution of these two molecules.[33] Field and co-workers investigated the reactions between iron(II) dihydride complexes and $CO_2$, COS, and $CS_2$ to produce the corresponding stable hydrido iron formates, hydrido iron thioformates, and hydrido iron dithioformates, respectively.[23]

Herein, we synthesized a water-soluble ruthenium hydride $[Ru(H)(bpy)_2(PTA)]PF_6$ (PTA = 1,3,5-triaza-7-phosphaadamantane) (**1a**) and directed our attention to the mechanism and kinetics studies of $CO_2$ and $CS_2$ insertions into the Ru−H bond of **1a** in a series of solvents (Scheme 1). For comparison purposes, we investigated the reactivity of $[Ru(H)(bpy)_2(PPh_3)]PF_6$ ($PPh_3$ = triphenylphosphine) (**1b**) with $CO_2$ and $CS_2$. The reactions between ruthenium hydride complexes and $CO_2$ and $CS_2$ produce stable ruthenium formates and ruthenium dithioformates, respectively (Scheme 1). Moreover, the reactivity of $CS_2$ toward ruthenium hydride complexes is higher than 1 to 3 orders of magnitude compared with $CO_2$. Notably, the relationship between the second order rate constant ($k_2$) of $CO_2$ insertion into ruthenium hydrides and the acceptor number (AN) of the solvents shows a linear correspondence between Ln($k_2$) and AN. The structures of ruthenium hydride complexes (**1a**, **1b**) and the ruthenium formate complex (**2b**) were confirmed by X-ray analysis.

**Scheme 1. Reactions of Ruthenium Hydrides**

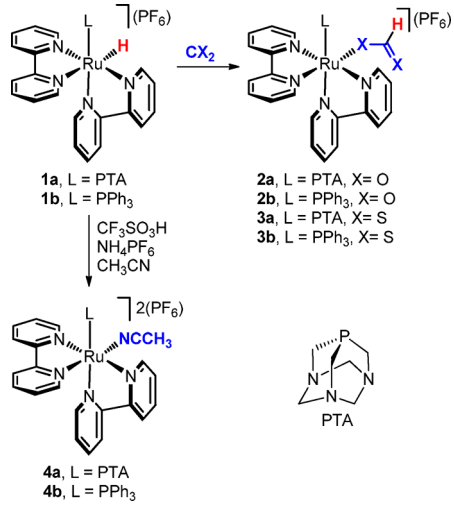



dx.doi.org/10.1021/ic500866d | Inorg. Chem. 2014, 53, 9570−9580

## EXPERIMENTAL SECTION

**Materials and Methods.** Unless otherwise stated, all starting materials were obtained from commercial sources and used without further purification. All synthetic work was carried out under an argon atmosphere using standard Schlenk techniques or a Vacuum Atmosphere drybox. The complexes were stored in a Vacuum Atmosphere drybox once isolated. For kinetic studies, acetonitrile was distilled over $P_2O_5$ and then over $CaH_2$ just before use. *N*,*N*-dimethylformamide (DMF) was dried over 4 Å molecular sieves and distilled at reduced pressure; methanol and acetone were dried over 4 Å molecular sieves and distilled under an argon atmosphere. PTA[57] and $Ru(bpy)_2Cl_2{\cdot}2H_2O$[58] were prepared according to the literature. $PPh_3$ and $CS_2$ were purchased from Alfa-Aesar (Tianjin, P. R. China). $CO_2$ (>99.999%) was obtained from Huate Co. Ltd. (Foshan, P. R. China).

UV−vis absorption spectra were recorded on a Shimadzu UV−1750 spectrometer. Elemental analysis was performed on Elementar Vairo EL. Some elemental analysis data of ruthenium complexes do not match with the theoretical values, owing to the presences of solvent molecules in the complex crystals (Supporting Information). The $^1$H NMR and $^{31}$P NMR spectra were recorded on Bruker AV III 400 at 25 °C. Infrared spectra were measured on a Bruker Tensor 27 FT−IR spectrometer with KBr pellets. X-ray crystallographic intensity data were collected for **1a**, **1b**, and **2b** using a Bruker-Siemens SMART AXS 1000 equipped with a CCD detector with graphite monochromated Mo K$\alpha$ radiation ($\lambda$ = 0.71073 Å). The structures were solved by the direct methods following Fourier syntheses and refined by the full−matrix least−squares method against $F^2$ using SHELXTL-97 software. The cyclic voltammetric measurements were performed on an ALS: CHI-660D electrochemical analyzer, with a glassy carbon working electrode, a Ag/AgCl (3 M aq. KCl) reference electrode, and a Pt counter electrode. The redox potentials of the complexes were measured in an acetonitrile solution containing tetra-*n*-butylammonium tetrafluoroborate (0.1 M) as the supporting electrolyte. The supporting electrolyte was dried under a vacuum at 100 °C for 3 days prior to use. The experimental electrochemical potentials were measured using a Ag/AgCl reference electrode (Ag/AgCl vs NHE = 197 mV).

**Preparation of Ruthenium Complexes.** *[Ru(H)(bpy)$_2$(PTA)]PF$_6$ (**1a**).* $Ru(bpy)_2Cl_2{\cdot}2H_2O$ (100 mg, 0.19 mmol), PTA (60 mg, 0.38 mmol), and $NaBH_4$ (110 mg, 2.85 mmol) in a mixture solution of ethanol (5 mL)−water (5 mL) were refluxed for 1 h under an Ar atmosphere. After cooling down to room temperature, an aqueous solution (3 mL) of $NH_4PF_6$ (156 mg, 0.95 mmol) was added, then the solution was evaporated to 8 mL under reduced pressure at room temperature to precipitate dark-red crystals of **1a**. The crystals were collected by filtration, washed with cold water, and dried in a vacuum. The product was further purified by recrystallization from acetonitrile and diethyl ether to give $[Ru(H)(bpy)_2(PTA)]PF_6{\cdot}0.25(CH_3CN){\cdot}0.5(Et_2O)$ (138 mg, yield 77%). $^1$H NMR (400 MHz, 25 °C, $CD_3CN$-$d_3$), $\delta$/ppm: 9.31−7.20 (m, 16H, bpy), 4.35−3.42 (m, 12H, PTA), −12.68 (d, 1H, Ru−H, $^2J_{H-P}$ = 24 Hz). $^{31}$P NMR (121.5 MHz, 25 °C, $CD_3CN$-$d_3$), $\delta$/ppm: −29.67 (d, PTA), −144.60 (heptet, $PF_6^-$). IR (KBr): $\nu$(Ru−H) = 1846 cm$^{-1}$. Anal. Calcd for $C_{28.5}H_{34.75}F_6N_{7.25}O_{0.5}P_2Ru$: C, 44.62; H, 4.55; N, 13.01. Found: C, 44.81; H, 4.59; N, 13.29%. The structure of **1a**·$CH_3CN$ was confirmed by an X-ray analysis (see Tables 3 and 4 and the Supporting Information for details).

*[Ru($\eta^1$-OC(H)=O)(bpy)$_2$(PTA)]PF$_6$ (**2a**).* A methanolic solution (100 mL) containing $[Ru(H)(bpy)_2(PTA)]PF_6$ (100 mg, 0.14 mmol) was bubbled with $CO_2$ at room temperature for about 2 h. The dark red solution turned to red brown. The solvent was then removed by a rotavapor under a vacuum. The product was recrystallized from acetonitrile and diethyl ether to give dark red crystals $[Ru(\eta^1\text{-}OC(H)=O)(bpy)_2(PTA)]PF_6$ (83 mg, yield 78%). $^1$H NMR (400 MHz, 25 °C, $CD_3CN$-$d_3$), $\delta$/ppm: 9.29 (d, 2H, OCHO and bpy), 8.39−7.15 (m, 15H, bpy), 4.40−3.78 (m, 12H, PTA). $^{31}$P NMR (121.5 MHz, 25 °C, $CD_3CN$-$d_3$), $\delta$/ppm: −40.69 (d, PTA), −144.61 (heptet, $PF_6^-$). IR (KBr): $\nu(OCO)_{asym}$ = 1618 cm$^{-1}$, $\nu(OCO)_{sym}$ = 1310 cm$^{-1}$. Anal. Calcd for $C_{27}H_{29}F_6N_7O_2P_2Ru$: C, 42.64; H, 3.84; N, 12.89. Found: C, 42.46; H, 4.15; N, 12.73%.

*[Ru($\eta^1$-SC(H)=S)(bpy)$_2$(PTA)]PF$_6$ (**3a**).* A dichloromethane solution (100 mL) containing $[Ru(H)(bpy)_2(PTA)]PF_6$ (100 mg, 0.14 mmol) was dropwise added to a dichloromethane solution (25 mL) of $CS_2$ (22 mg, 0.28 mmol) for 30 min at room temperature. Then, the purple solution turned to red brown. The solvent and excess $CS_2$ were then removed by a rotavapor under a vacuum. The product was recrystallized from acetonitrile and diethyl ether to give red brown crystals $[Ru(\eta^1\text{-}SC(H)=S)(bpy)_2(PTA)]PF_6$ (80 mg, yield 72%). $^1$H NMR (400 MHz, 25 °C, $CD_3CN$-$d_3$), $\delta$/ppm: 10.86 (s, 1H, SCHS), 9.37 (s, 1H, bpy), 9.10 (s, 1H, bpy), 8.37−7.30 (m, 14H, bpy), 4.41−3.80 (m, 12H, PTA). $^{31}$P NMR (121.5 MHz, 25 °C, $CD_3CN$-$d_3$), $\delta$/ppm: −41.68 (s, PTA), −144.61 (heptet, $PF_6^-$). IR (KBr): $\nu(SCS)_{as}$ = 989 cm$^{-1}$. Anal. Calcd for $C_{27}H_{29}F_6N_7P_2RuS_2$: C, 40.91; H, 3.69; N, 12.37; S, 8.09. Found: C, 40.24; H, 3.65; N, 12.07; S, 7.63%. The presence of diethyl ether molecules in the complex crystals was confirmed by $^1$H NMR analysis.

*[Ru(NCCH$_3$)(bpy)$_2$(PTA)](PF$_6$)$_2$ (**4a**).* An acetonitrile solution (8 mL) of $[Ru(H)(bpy)_2(PTA)]PF_6$ (100 mg, 0.14 mmol) was cooled to 0 °C. To this solution, an excess amount of $CF_3SO_3H$ (78 mg, 0.52 mmol) was added. The reaction mixture was stirred at 0 °C for 10 min and then at room temperature for another 30 min. After the reaction, the solvent was reduced to 2 mL under reduced pressure, and the mixture was treated with an aqueous solution (5 mL) of $NH_4PF_6$ (106 mg, 0.65 mmol). By stirring the resulting solution, a yellow solid separated out, which was filtered and crystallized from acetone and diethyl ether to give a yellow powder $\{[Ru(NCCH_3)(bpy)_2(PTA)](PF_6)_2\}{\cdot}0.5(Et_2O)$ (103 mg, yield 82%). $^1$H NMR (400 MHz, 25 °C, $CD_3CN$-$d_3$), $\delta$/ppm: 9.18−7.27 (m, 16H, bpy), 4.72−3.44 (m, 12H, PTA), 2.30 (s, 3H, $CH_3CN$). $^{31}$P NMR (121.5 MHz, 25 °C, $CD_3CN$-$d_3$), $\delta$/ppm: −27.23 (s, PTA), −144.58 (heptet, $PF_6^-$). Anal. Calcd for $C_{30}H_{36}F_{12}N_8O_{0.5}P_3Ru$: C, 38.39; H, 3.87; N, 11.94. Found: C, 38.74; H, 3.73; N, 11.57%.

*[Ru(H)(bpy)$_2$(PPh$_3$)]PF$_6$ (**1b**).* $Ru(bpy)_2Cl_2{\cdot}2H_2O$ (100 mg, 0.19 mmol), $PPh_3$ (150 mg, 0.57 mmol), and $NaBH_4$ (110 mg, 2.85 mmol) in a mixture solution of ethanol (10 mL)−water (5 mL) were refluxed for 1 h under an Ar atmosphere. After cooling down to room temperature, an aqueous solution (3 mL) of $NH_4PF_6$ (156 mg, 0.95 mmol) was added, then the solution was evaporated to 8 mL under reduced pressure at room temperature to precipitate dark-brown crystals of **1b.** The crystals were collected by filtration, washed with cold water, and dried in a vacuum. The product was recrystallized from acetonitrile and diethyl ether to give $\{[Ru(H)(bpy)_2(PPh_3)]PF_6\}{\cdot}0.5(Et_2O)$ (140 mg, yield 86%). $^1$H NMR (400 MHz, 25 °C, $CD_3CN$-$d_3$), $\delta$/ppm: 8.65−6.84 (m, 31H, Ph and bpy), −12.10 (d, 1H, Ru−H, $^2J_{H-P}$ = 24 Hz). $^{31}$P NMR (121.5 MHz, 25 °C, $CD_3CN$-$d_3$), $\delta$/ppm: 66.80 (s, $PPh_3$), −144.64 (heptet, $PF_6^-$). IR (KBr): $\nu$(Ru−H) = 1911 cm$^{-1}$. Anal. Calcd for $C_{40}H_{37}F_6N_4P_2RuO_{0.5}$: C, 55.94; H, 4.34; N, 6.52. Found: C, 54.60; H, 4.15; N, 6.48%.

*[Ru($\eta^1$-OC(H)=O)(bpy)$_2$(PPh$_3$)]PF$_6$ (**2b**).* **2b** was prepared with reaction conditions similar to that of **2a**. **2b** was purified by recrystallization from acetonitrile and diethyl ether to give dark red crystals $\{[Ru(\eta^1\text{-}OC(H)=O)(bpy)_2(PPh_3)]PF_6\}_3{\cdot}(CH_3CN)_2{\cdot}(Et_2O)$ (56 mg, yield 50%). $^1$H NMR (400 MHz, 25 °C, $CD_3CN$-$d_3$), $\delta$/ppm: 9.21 (d, 1H, OCHO), 9.08 (d, 1H, bpy), 8.32−6.77 (m, 30H, Ph and bpy). $^{31}$P NMR (121.5 MHz, 25 °C, $CD_3CN$-$d_3$), $\delta$/ppm: 44.54 (s, $PPh_3$), −144.47 (heptet, $PF_6^-$). IR (KBr): $\nu(OCO)_{asym}$ = 1620 cm$^{-1}$, $\nu(OCO)_{sym}$ = 1310 cm$^{-1}$. Anal. Calcd for $C_{125}H_{112}F_{18}N_{14}O_7P_6Ru_3$: C, 54.53; H, 4.10; N, 7.12. Found: C, 54.17; H, 4.02; N, 7.16%. The structure of **2b**·0.25$CH_3CN$ was confirmed by an X-ray analysis (see Tables 3 and 4 and the Supporting Information for details).

*[Ru($\eta^1$-SC(H)=S)(bpy)$_2$(PPh$_3$)]PF$_6$ (**3b**).* **3b** was prepared with reaction conditions similar to that of **3a**. **3b** was purified by recrystallization from acetonitrile and diethyl ether to give $[Ru(\eta^1\text{-}SC(H)=S)(bpy)_2(PPh_3)]PF_6$ (80 mg, yield 70%). $^1$H NMR (400 MHz, 25 °C, $CD_3CN$-$d_3$), $\delta$/ppm: 10.82 (s, 1H, SCHS), 9.21 (d, 1H, bpy), 8.70 (d, 1H, bpy), 8.45−6.93 (m, 29H, Ph and bpy). $^{31}$P NMR (121.5 MHz, 25 °C, $CD_3CN$-$d_3$), $\delta$/ppm: 43.97 (s, $PPh_3$), −144.61 (heptet, $PF_6^-$). IR (KBr): $\nu(SCS)_{as}$ = 978 cm$^{-1}$. Anal. Calcd for


dx.doi.org/10.1021/ic500866d | Inorg. Chem. 2014, 53, 9570−9580

$C_{39}H_{32}F_6N_4P_2RuS_2$: C, 52.17; H, 3.59; N, 6.24; S, 7.14. Found: C, 51.66; H, 3.37; N, 6.36; S, 6.51%. The presence of diethyl ether molecules in the complex crystals was confirmed by $^1$H NMR analysis.

*[Ru(NCCH$_3$)(bpy)$_2$(PPh$_3$)](PF$_6$)$_2$ (**4b**).* **4b** was prepared with reaction conditions similar to that of **4a**. **4b** was purified by recrystallization from acetonitrile and diethyl ether to give a brown powder $[Ru(NCCH_3)(bpy)_2(PPh_3)](PF_6)_2$ (91 mg, yield 74%). $^1$H NMR (400 MHz, 25 °C, $CD_3CN$-$d_3$), $\delta$/ppm: 9.00 (d, 1H, $J$ = 4 Hz), 8.55−7.02 (m, 30H, bpy and $PPh_3$), 2.26 (s, 3H, $CH_3CN$). $^{31}$P NMR (121.5 MHz, 25 °C, $CD_3CN$-$d_3$), $\delta$/ppm: 44.34 (s, $PPh_3$). Anal. Calcd for $C_{40}H_{34}F_{12}N_5P_3Ru$: C, 47.72; H, 3.40; N, 6.96. Found: C, 47.87; H, 3.16; N, 7.15%.

**Typical Procedure for Kinetic Studies.** *Reaction with CO$_2$.* An acetonitrile solution (3 mL) of **1a** ($1 \times 10^{-4}$−$5 \times 10^{-4}$ M) in a quartz cubic cell (5 mL) was gently bubbled with Ar for 20 min and then sealed with a rubber septum. A 50−200 $\mu$L of $CO_2$−saturated solution was added into the cell using a gas−tight syringe. The UV−Vis absorption data at the selected wavelength were recorded every 1−10 s with air as a blank. The color of the solution changed from pink to orange. The formation of **2a** was confirmed by NMR.

*Reaction with CS$_2$.* An acetonitrile solution (3 mL) of **1a** [$(1 \times 10^{-4})$−$(5 \times 10^{-4})$ M] in a quartz cubic cell (5 mL) was gently bubbled with Ar for 20 min and then sealed with a rubber septum. A 20−100 $\mu$L of $CS_2$ (0.1 M) solution was added into the cell using a gastight syringe. The UV−vis absorption data at the selected wavelength were recorded every 1−10 s. The color of the solution changed from pink to orange. The formation of **3a** was confirmed by NMR.

**Saturated Concentration of CO$_2$.** The $CO_2$-saturated solution was obtained by gently bubbling $CO_2$ into a 5.0 mL solvent in a reaction vessel of 8.0 mL capacity for 20 min. The saturated concentrations of $CO_2$ in various solvents at 25 °C were referred to the references.[17,59,60] Solubility value: $CO_2$/MeOH (0.14 M atm$^{-1}$), $CO_2$/$CH_3CN$ (0.29 M atm$^{-1}$), $CO_2$/DMF (0.20 M atm$^{-1}$), $CO_2$/acetone (0.29 M atm$^{-1}$)

## RESULTS AND DISCUSSION

**Ruthenium Hydride Complexes.** Treatment $Ru(bpy)_2Cl_2{\cdot}2H_2O$ with a phosphine ligand PTA in the presence of $NaBH_4$ gave a ruthenium hydride cation $[Ru(H)(bpy)_2(PTA)]^+$ which was isolated as a $PF_6$ salt of **1a**. **1b** was prepared following the same synthetic procedure as for **1a** except that the PTA was replaced by a $PPh_3$.[61] The ruthenium hydride complexes **1a** and **1b** are dark-purple solids and moderately stable in air and in a solution of polar organic solvent. Moreover, **1a** is moderately soluble in water. The $^1$H NMR spectra of **1a** and **1b** exhibit characteristic low frequency doublets at −12.6 ($^2J_{PH}$ = 32 Hz) and −12.1 ppm ($^2J_{PH}$ = 32 Hz), respectively, which are attributed to the resonances of Ru−H due to the coupling with the phosphorus nuclei (Table 1). FT-IR spectra of **1a** and **2a** show the vibrations of Ru−H at 1846 and 1911 cm$^{-1}$, respectively (Table 1).

Bipyridine containing complexes normally exhibit metal-to-ligand charge-transfer (MLCT) bands at relatively low energy. Table 2 shows the UV−vis electronic absorption of the complexes **1a**−**4b** in $CH_3CN$ at 25 °C. Continuous bubbling of $CO_2$ into an acetonitrile solution of **1a** caused the hypsochromic shift of the absorption maximum from 514 to 473 nm, indicating the reaction of the hydrido complex with $CO_2$. Figure 1a shows the spectral changes for the reaction of **1a** and $CO_2$ in acetonitrile regulated in a thermostated cell holder under 1 atm of Ar at 25 °C, and the UV−vis spectra were recorded every 4 min with air as the blank. There is a strong absorbance band from 400 to 600 nm of **1a** with a maximum at 514 nm. This absorption maximum, however, shifted to 473 nm after the $CO_2$ insertion reaction. Moreover, the color of the acetonitrile solution accordingly changed from pink to orange (Figure 1b). Similar spectral and color changes were also observed when the reactions were performed in water, methanol, acetone, and DMF. In addition to **1a**, the ruthenium hydride **1b** was subjected to the reaction conditions for comparison purposes. However, we found that **1b** reacted with $CO_2$ in acetonitrile with a relatively slower rate than that of **1a**. Similarly, after the reaction of $CO_2$ and **1b**, the color of the solution changed from pink to orange. The similar spectral and color changes were also observed when the reactions of **1b** and $CO_2$ were performed in the solvents of methanol, acetone, and DMF.

In addition to $CO_2$ reduction, the $CS_2$ insertions into the Ru hydride complexes were performed in acetonitrile solution in the experiment. Similarly, a hypsochromic shift of the absorption maximum can be observed when dropping a $CS_2$ solution into **1a**. Figure 1c shows spectral changes after the treatment of **1a** with $CS_2$ in acetonitrile under Ar at 25 °C. The maximum absorption shifted from 514 to 425 nm after the reaction, which is much more evident than the reaction of **1a** with $CO_2$.

After the $CO_2$ and $CS_2$ insertion reactions, the corresponding formate complexes (**2a** and **2b**, Scheme 1) and dithioformate complexes (**3a** and **3b**, Scheme 1) can be isolated from the solutions. The formations of formate complexes and dithioformate complexes were confirmed by $^1$H NMR, $^{31}$P NMR, and FT-IR (Supporting Information); the structures of several ruthenium complexes were further confirmed by an X-ray analysis (will be discussed below). In the $^1$H NMR spectra of formate and dithioformate complexes, the signals of Ru−H were unobserved. The resonances of the proton in the $\eta^1$-OC(H)=O group for formate complexes appeared at 7.86 ppm for **2a** and 8.03 ppm for **2b**, whereas the signals of the

**Table 1. Summary of $^1$H, $^{31}$P NMR and FT-IR Data for Complexes 1a−3b**

| | NMR [$\delta$, ppm] | | | IR [cm$^{-1}$] | |
|---|---|---|---|---|---|
| | $^1$H | | | | |
| complex | hydride | formate | $^{31}$P | $\nu$(Ru−H) | $\nu$(CX$_2$) |
| **1a** | −12.6 | | −29.7 | 1846 | |
| **1b** | −12.1 | | 66.8 | 1911 | |
| **2a** | | 7.86 | −40.7 | | $\nu(CO_2)_s$ 1310, $\nu(CO_2)_{as}$ 1618 |
| **2b** | | 8.03 | 44.5 | | $\nu(CO_2)_s$ 1310, $\nu(CO_2)_{as}$ 1620 |
| **3a** | | 10.86 | −41.7 | | $\nu$(HCS) 1236, $\nu(CS_2)_{as}$ 989 |
| **3b** | | 10.82 | 43.97 | | $\nu$(HCS) 1242, $\nu(CS_2)_{as}$ 978 |

**Table 2. UV−Vis Electronic Absorption Spectra of the Complexes in $CH_3CN$ under Ar at 25 °C**

| compound | $\lambda_{max}$, nm ($\varepsilon$, M$^{-1}$ cm$^{-1}$) |
|---|---|
| **1a** | 245 ($2.48 \times 10^4$), 295 ($4.49 \times 10^4$), 354($8.24 \times 10^3$), 514 ($7.96 \times 10^3$) |
| **2a** | 244 ($2.06 \times 10^4$), 292 ($3.83 \times 10^4$), 466 ($5.99\times 10^3$), 473 ($5.99\times 10^3$) |
| **3a** | 243 ($2.16 \times 10^4$), 291 ($3.43 \times 10^4$), 425 ($6.34 \times 10^3$) |
| **4a** | 243 ($1.81 \times 10^4$), 286 ($3.47 \times 10^4$), 416 ($5.66 \times 10^3$) |
| **1b** | 295 ($4.55 \times 10^4$), 346 ($8.90 \times 10^3$), 497 ($7.38 \times 10^3$) |
| **2b** | 291 ($3.94 \times 10^4$), 448 ($6.21 \times 10^3$) |
| **3b** | 290 ($3.68 \times 10^4$), 424 ($6.05 \times 10^3$) |
| **4b** | 284 ($3.93 \times 10^4$), 404 ($7.47 \times 10^3$) |


dx.doi.org/10.1021/ic500866d | Inorg. Chem. 2014, 53, 9570−9580

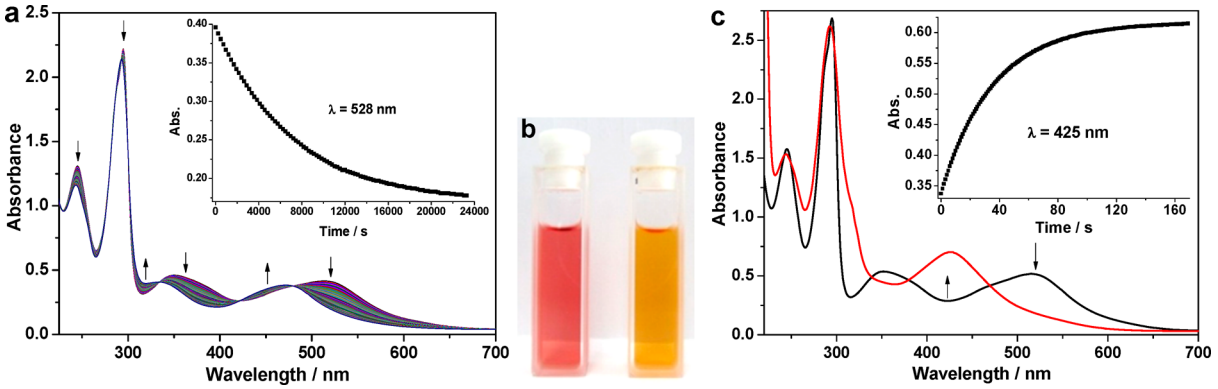


**Figure 1.** (a) UV−vis spectral changes of reaction between **1a** ($5.86 \times 10^{-5}$ M) and $CO_2$ ($1.81 \times 10^{-2}$ M) in $CH_3CN$ under Ar at 25 °C [inset, the absorbance changes at 528 nm]. (b) **1a** in $CH_3CN$ before (pink) and after (orange) the reaction with $CO_2$. (c) UV−vis spectral changes of reaction between **1a** ($5.40 \times 10^{-5}$ M) and $CS_2$ ($2.90 \times 10^{-3}$ M) in $CH_3CN$ under Ar at 25 °C [inset, the absorbance changes at 425 nm].

**Table 3. Crystallographic Data and Structural Refinement of 1a, 1b, and 2b**

| | $[Ru(H)(bpy)_2(PTA)]PF_6{\cdot}CH_3CN$, **1a**·$CH_3CN$ | $[Ru(H)(bpy)_2(PPh_3)]PF_6$, **1b** | $[Ru(\eta^1\text{-}OC(H)=O)(bpy)_2(PPh_3)]PF_6{\cdot}0.25CH_3CN$, **2b**·$0.25CH_3CN$ |
|---|---|---|---|
| formula | $C_{28}H_{31}F_6N_8P_2Ru$ | $C_{38}H_{32}RuF_6N_4P_2$ | $C_{39.5}H_{32.75}RuF_6N_{4.25}O_2P_2$ |
| $M_w$ | 757.63 | 821.69 | 875.96 |
| $T$/K | 113 | 113 | 113 |
| cryst syst | monoclinic | triclinic | monoclinic |
| space group | $P21/c$ | $P\bar{1}$ | $P21/c$ |
| $a$/Å | 14.234(2) | 14.617(3) | 10.063(4) |
| $b$/Å | 14.649(2) | 14.713(3) | 15.083(6) |
| $c$/Å | 14.371(2) | 16.966(3) | 27.02(1) |
| $\alpha$/deg | 90 | 77.737 | 90 |
| $\beta$/deg | 93.162(2) | 86.071 | 110.915 |
| $\gamma$/deg | 90 | 76.882 | 90 |
| $V$/Å$^3$ | 2992.0(7) | 3471(6) | 3831(3) |
| $Z$ | 4 | 4 | 4 |
| calculated density/g cm$^{-3}$ | 1.682 | 1.572 | 1.519 |
| $\mu$/mm$^{-1}$ | 0.704 | 0.611 | 0.563 |
| $F$(0 0 0) | 1536.0 | 1664 | 1774.0 |
| $\theta$ range (deg) | 1.43−27.87 | 1.43−27.87 | 1.57−27.97 |
| reflns. collected | 30124 | 35556 | 38049 |
| ind. reflns. | 7136 [$R$(int) = 0.0342] | 16 559 [$R$(int) = 0.0376] | 9148 [$R$(int) = 0.0562] |
| data/restr./params | 7136/0/411 | 16559/0/927 | 9148/147/555 |
| Final $R$ indices [$I > 2\sigma(I)$] | R1 = 0.0247, wR2 = 0.0669 | R1 = 0.0427, wR2 = 0.0987 | R1 = 0.0539, wR2 = 0.1206 |
| $R$ indices (all data) | R1 = 0.0288, wR2 = 0.0687 | R1 = 0.0539, wR2 = 0.1048 | R1 = 0.0633, wR2 = 0.1154 |
| goodness-of-fit on $F^2$ | 0.972 | 0.980 | 1.137 |

proton in the $\eta^1$-SC(H)=S group for dithioformate complexes were observed at 10.86 ppm for **3a** and 10.82 ppm for **3b** (Table 1). FT-IR spectra of both **2a** and **2b** show the symmetric and asymmetric stretching vibrations of the $\eta^1$-OC(H)=O group at 1310 and 1618 cm$^{-1}$, respectively, which is typically in the region of the $\eta^1$-formato ligand (Table 1). Asymmetric stretching vibrations of the $\eta^1$-SC(H)=S group in dithioformate complexes **3a** and **3b** showed absorption at 989 and 978 cm$^{-1}$, respectively. Generally, the FT-IR absorption of the $\eta^1$-dithioformato ligand appeared at 980−1012 cm$^{-1}$, whereas the $\eta^2$-dithioformato ligand appeared at 900−960 cm$^{-1}$.[23,53] The above results suggested that both the $\eta^1$-OC(H)=O and $\eta^1$-SC(H)=S ligands in $[Ru(\eta^1\text{-}XC(H)=X)(bpy)_2(L)]^+$ (X = O and S, L = PTA and $PPh_3$) complexes can bind to the Ru atom in an $\eta^1$-fashion through the O and S atom, respectively. The summary of $^1$H NMR, $^{31}$P NMR, and FT-IR data for the complexes **1a**−**3b** is displayed in Table 1.

**Crystal Structures of 1a, 1b, and 2b.** X-ray crystallographic intensity data were collected for **1a**, **1b**, and **2b** using a Bruker-Siemens SMART AXS 1000 equipped with a CCD detector with graphite monochromated Mo K$\alpha$ radiation ($\lambda$ = 0.71073 Å). The single-crystal X-ray diffraction reveals that **1a** crystallizes in a monoclinic space group $P21/c$, whereas **1b** in a triclinic space group $P\bar{1}$ (Table 3). As shown in Figure 2a and b, the Ru(II) ions are coordinated to two bpy ligands, one phosphine ligand and a hydride ion in a distorted octahedral geometry in both **1a** and **1b**. Moreover, two bpy ligands are *cis* to one another in both **1a** and **1b**; the distances of Ru−N bonds ranged from 2.04 to 2.18 Å. The Ru−P bonds in **1a** and **1b** are 2.26 and 2.28 Å, respectively, whereas the Ru−H bonds are 1.727 Å for **1a** and 1.58 Å for **1b**. In **1a**, the asymmetry unit


dx.doi.org/10.1021/ic500866d | Inorg. Chem. 2014, 53, 9570−9580

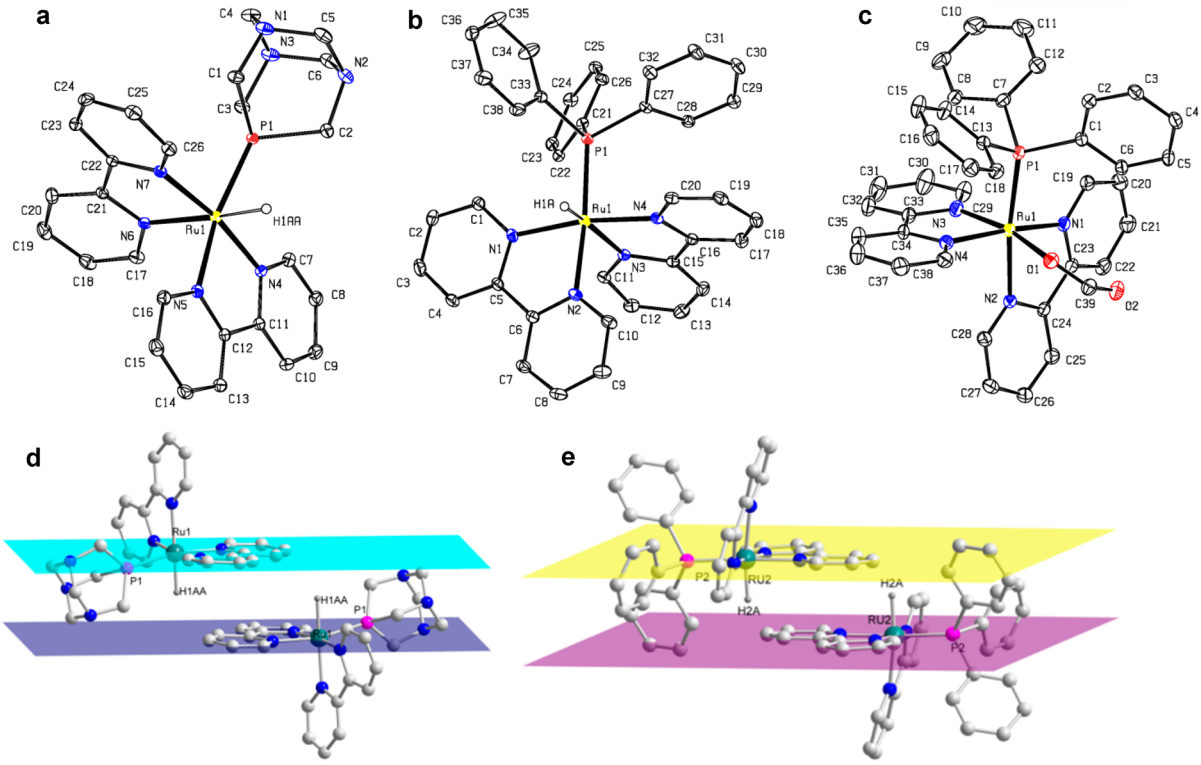


**Figure 2.** ORTEP drawing of (a) $[Ru(H)(bpy)_2(PTA)]^+$, (b) $[Ru(H)(bpy)_2(PPh_3)]^+$, and (c) $[Ru(\eta^1\text{-}OC(H)=O)(bpy)_2(PPh_3)]^+$ with all ellipsoids at 30% probability. $\pi$-stacking forms of two $[Ru(H)(bpy)_2(PTA)]^+$ (d) and $[Ru(H)(bpy)_2(PPh_3)]^+$ (e) units. All hydrogen atoms, except that attached to ruthenium in the hydride complexes, are omitted for clarity.

**Table 4. Selected Bond Lengths (Å) and Angles (deg) for 1a, 1b, and 2b**

| $[Ru(H)(bpy)_2(PTA)](PF_6)\cdot CH_3CN$, **1a**·$CH_3CN$ | | $[Ru(H)(bpy)_2(PPh_3)](PF_6)$, **1b** | | $[Ru(\eta^1\text{-}OC(H)=O)(bpy)_2(PPh_3)]PF_6\cdot 0.25CH_3CN$, **2b**·$0.25CH_3CN$ | |
|---|---|---|---|---|---|
| bond lengths | | bond lengths | | bond lengths | |
| Ru(1)−H(1AA) | 1.727(19) | Ru(1)−H(1A) | 1.58(3) | Ru(1)−O(1) | 2.114(2) |
| Ru(1)−N(4) | 2.0645(13) | Ru(1)−P(1) | 2.2894(8) | Ru(1)−P(1) | 2.3253(11) |
| Ru(1)−N(7) | 2.0706(13) | Ru(1)−N(4) | 2.049(2) | Ru(1)−N(3) | 2.050(3) |
| Ru(1)−N(5) | 2.0963(13) | Ru(1)−N(1) | 2.077(2) | Ru(1)−N(4) | 2.066(3) |
| Ru(1)−N(6) | 2.1369(13) | Ru(1)−N(2) | 2.097(2) | Ru(1)−N(1) | 2.091(3) |
| Ru(1)−P(1) | 2.2631(5) | Ru(1)−N(3) | 2.181(2) | Ru(1)−N(2) | 2.095(3) |
| | | | | O(1)−C(39) | 1.267(4) |
| | | | | O(2)−C(39) | 1.224(4) |
| | | | | C(39)−H(39) | 0.982(10) |
| bond angles | | bond angles | | bond angles | |
| N(4)−Ru(1)−N(7) | 170.61(5) | N(4)−Ru(1)−N(1) | 170.74(8) | Ru(1)−O(1)−C(39) | 125.8(2) |
| N(4)−Ru(1)−N(5) | 77.81(5) | N(4)−Ru(1)−N(2) | 93.24(8) | O(2)−C(39)−O(1) | 128.8(3) |
| N(7)−Ru(1)−N(5) | 96.12(5) | N(1)−Ru(1)−N(2) | 77.75(9) | O(2)−C(39)−H(39) | 117(2) |
| N(4)−Ru(1)−N(6) | 95.51(5) | N(4)−Ru(1)−N(3) | 76.99(8) | O(1)−C(39)−H(39) | 114(2) |
| N(7)−Ru(1)−N(6) | 77.17(5) | N(1)−Ru(1)−N(3) | 99.56(8) | N(3)−Ru(1)−N(4) | 79.55(13) |
| N(5)−Ru(1)−N(6) | 89.91(5) | N(2)−Ru(1)−N(3) | 83.01(8) | N(3)−Ru(1)−N(1) | 90.92(12) |
| N(4)−Ru(1)−P(1) | 99.34(4) | N(4)−Ru(1)−P(1) | 90.76(6) | N(4)−Ru(1)−N(1) | 167.14(12) |
| N(7)−Ru(1)−P(1) | 88.09(4) | N(1)−Ru(1)−P(1) | 98.37(6) | N(3)−Ru(1)−N(2) | 90.79(12) |
| N(5)−Ru(1)−P(1) | 167.65(4) | N(2)−Ru(1)−P(1) | 174.73(6) | N(4)−Ru(1)−N(2) | 93.23(11) |
| N(6)−Ru(1)−P(1) | 102.35(4) | N(3)−Ru(1)−P(1) | 101.26(6) | N(1)−Ru(1)−N(2) | 78.16(11) |
| N(4)−Ru(1)−H(1AA) | 93.0(6) | N(4)−Ru(1)−H(1A) | 93.3(11) | N(3)−Ru(1)−O(1) | 167.22(11) |
| N(7)−Ru(1)−H(1AA) | 93.9(6) | N(1)−Ru(1)−H(1A) | 88.2(11) | | |
| N(5)−Ru(1)−H(1AA) | 87.9(6) | N(2)−Ru(1)−H(1A) | 85.5(11) | | |
| N(6)−Ru(1)−H(1AA) | 170.5(6) | N(3)−Ru(1)−H(1A) | 164.4(12) | | |
| P(1)−Ru(1)−H(1AA) | 80.2(6) | P(1)−Ru(1)−H(1A) | 90.9(11) | | |


dx.doi.org/10.1021/ic500866d | Inorg. Chem. 2014, 53, 9570−9580

consists of four **1a**·$CH_3CN$ units; two adjacent units interact with one another through a $\pi$-stacking interaction of two bpy ligands (Figure 2d). The two bpy ligands are parallel with each other with an average distance between planes of 3.372 Å. In **1b**, two Ru2 units in two adjacent asymmetry units interact with one another through a $\pi$-stacking interaction of two bpy ligands (Figure 2e). The two bpy ligands are parallel with each other with a distance between two planes of 3.385 Å. Six F atoms of the $PF_6^-$ anion were bonded to hydrogen atoms from $PPh_3$ and bpy ligands of six $[Ru(H)(bpy)_2(PPh_3)]^+$ cations; H···F distances ranged from 2.452 to 2.600 Å. Moreover, the asymmetry unit consists of four **1b** units. Ru1 and Ru2 cations are pseudosymmetric; they adopt the same coordination mode but do not coincident with each other completely (Figure 2e).

**2b** crystallizes in monoclinic space group $P21/c$, also a distorted octahedral geometry (Figure 2c). The ruthenium(II) ion is bonded to two bpy ligands, one $PPh_3$ ligand, and one $\eta^1$-OC(H)=O ligand (Ru−N 2.05−2.09 Å; Ru−P 2.32 Å; Ru−O 2.11 Å; ∠O−C−O 128.9°). The two bpy ligands are *cis* to one another; the formato ligand is in an $\eta^1$-fashion to the metal. The asymmetry unit consists of four **2b** units and one acetonitrile molecule. F1, F2, F3, and F4 atoms of hexafluorophosphate group, and all the atoms of acetonitrile molecules are disordered crystallographically at two positions. The crystallographic data, structural refinement, and selected bond lengths and angles of **1a**, **1b**, and **2b** were described in Tables 3 and 4.

**Electrochemistry.** The acetonitrile complexes **4a** and **4b** were prepared by treatment of the hydride complexes **1a** and **1b**, respectively, with an excess amount of acid in acetonitrile solution (Scheme 1). For comparison purposes, both acetonitrile complexes (**4a** and **4b**) and hydride complexes (**1a** and **1b**) were subjected to electrochemistry analysis. Figure 3 illustrates the cyclic voltammograms of **1a**, **4a**, **1b**, and **4b** in an acetonitrile solution in a potential range of 2 to −2 V using a Ag/AgCl reference electrode (Ag/AgCl vs NHE = 197 mV). In the case of **1a** and **4a**, the reduction process for the acetonitrile complex $[Ru(NCCH_3)(bpy)_2(PTA)]^{2+}$ has a large peak separation which was also observed in its corresponding hydride complex $[Ru(H)(bpy)_2(PTA)]^+$, but it occurs at considerably more positive potential compared with $[Ru(H)(bpy)_2(PTA)]^+$. The anodic oxidation of $[Ru(H)(bpy)_2(PTA)]^+$ irreversibly occurred at 0.5 V to give the corresponding acetonitrile complex $[Ru(NCCH_3)(bpy)_2(PTA)]^{2+}$. The electrochemical formation of $[Ru(NCCH_3)(bpy)_2(PTA)]^{2+}$ should proceed via a sequential loss of two electrons and a proton from $[Ru(H)(bpy)_2(PTA)]^+$ followed by the coordination of a solvent molecule.[14,17] $[Ru(NCCH_3)(bpy)_2(PTA)]^{2+}$ is oxidized irreversibly with the potential exceeding 1.5 V. Similarly, the anodic oxidation of $[Ru(H)(bpy)_2(PPh_3)]^+$ irreversibly occurred at 0.7 V to give the corresponding acetonitrile complex $[Ru(NCCH_3)(bpy)_2(PPh_3)]^{2+}$. Moreover, the reversible conversion of $[Ru(NCCH_3)(bpy)_2(PPh_3)]^{2+}$ and $[Ru(NCCH_3)(bpy)_2(PPh_3)]^{3+}$ appeared at 1.5 V.

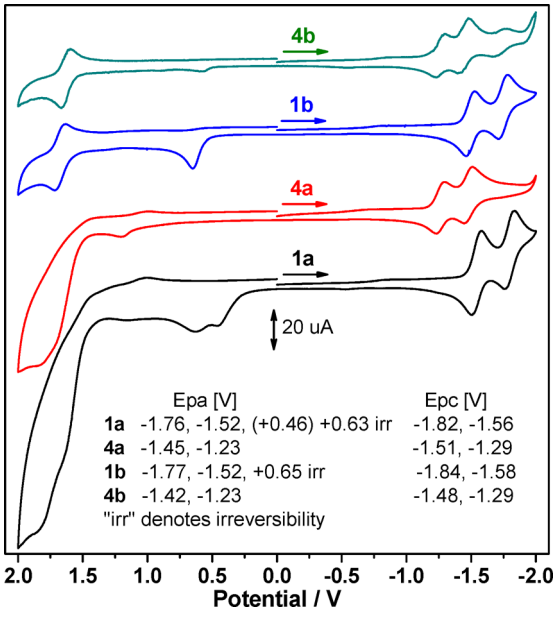


**Figure 3.** Cyclic voltammograms (CV) of **1a**, **4a**, **1b**, and **4b** (1.0 mM) under Ar in $CH_3CN$ [$Bu_4NBF_4$, (0.1 M in $CH_3CN$); scan rate, 100 mV $s^{-1}$; reference electrode, AgCl/Ag (3 M aqueous KCl); counter electrode, platinum wire; working electrode, glassy carbon ($d$ = 3 mm)].

**Kinetics Studies.** Current research results show that the reaction of the ruthenium hydride with $CO_2$ obeys a second-order process.[16,17] The rate of ruthenium formate complex formation ($r$[RuOCHO]) can be expressed as the following equation as a second order reaction:

$$r[\mathrm{RuOCHO}] = \frac{d[\mathrm{RuH}]}{dt} = \frac{d[\mathrm{RuOCHO}]}{dt} = k_2[\mathrm{CO_2}][\mathrm{RuH}] = k_{obs}[\mathrm{RuH}]$$

$$k_{obs} = k_2[\mathrm{CO_2}]$$

$$\mathrm{Ln}(A_0 - A) = k_{obs}t$$

Moreover, this process can be simplified as a pseudo-first-order reaction under the condition that an appropriate excess amount of $CO_2$ is used in the reaction system.[14,16,17,24] [RuOCHO], [$CO_2$], and [RuH] indicate molar concentrations of a ruthenium formate complex, $CO_2$, and a ruthenium hydride complex, respectively; whereas $k_2$ is the second order rate constant of $CO_2$ insertion into ruthenium hydride at a certain temperature, $k_{obs}$ is the simplified pseudo-first-order rate constant for ruthenium formate complex formation at a certain temperature. Moreover, $k_{obs}$ equals $k_2$ times [$CO_2$]. $A_0$ and A donate initial and specific concentration/absorbance of RuH, respectively.

The kinetics of $CO_2$ insertions into ruthenium hydride complexes were performed in different solvents, including methanol, acetonitrile, DMF, and acetone. The progress of the reaction was followed by UV−vis absorption spectra. Owing to the solvent effect, suitable wavelength was selected for the reactions in different solvents. Figure 4a shows the UV−vis absorption changes of **1a** with excess $CO_2$ at the selected wavelength of 528 nm in $CH_3CN$ solution; these data were recorded every 1 s with air as blank under 1 atm of Ar at 25 °C. Table 5 shows the initial concentrations of **1a** and $CO_2$ for Figure 4a generation and the obtained $k_{obs}$ from Figure 4a for the reaction of **1a** and $CO_2$.

Therefore, the apparent first order rate constant ($k_{obs}$) for $CO_2$ insertion into **1a** was obtained from Figure 4a and


dx.doi.org/10.1021/ic500866d | Inorg. Chem. 2014, 53, 9570−9580

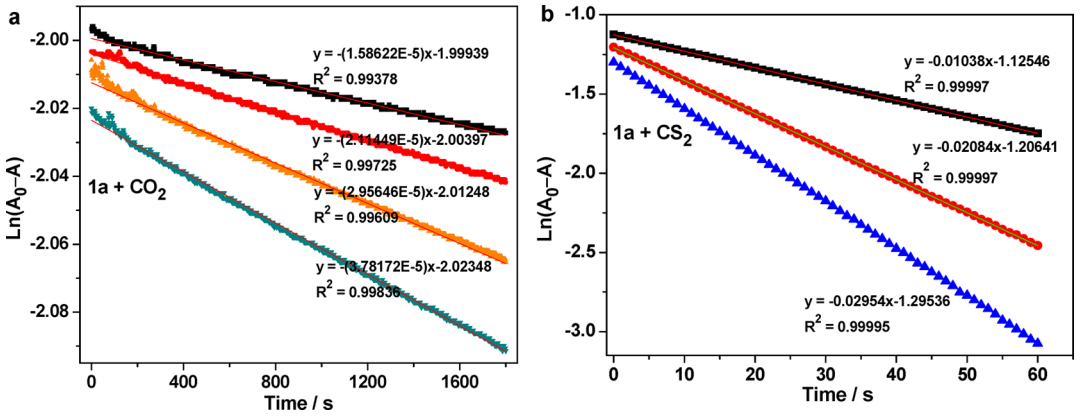


**Figure 4.** (a) The decay of UV−vis absorption of **1a** with excess $CO_2$ at the selected wavelength of 528 nm in $CH_3CN$ solution under 1 atm of Ar at 25 °C (the data were recorded every 1 s with air as blank). (b) The decay of UV−vis absorption of **1a** with excess $CS_2$ at the selected wavelength of 425 nm in $CH_3CN$ solution under 1 atm of Ar at 25 °C (the data were recorded every 1 s with air as blank).

**Table 5. Initial Concentrations of 1a, $CO_2$, and $CS_2$, the Simplified Pseudo-First-Order Rate Constant ($k_{obs}$) and the Obtained Second-Order Rate Constants ($k_2$) for the Reaction of 1a with $CO_2$ and $CS_2$ in $CH_3CN$ under 1 atm of Ar at 25 °C**

| **1a** + $CO_2$ | | | | **1a** + $CS_2$ | | | |
|---|---|---|---|---|---|---|---|
| [**1a**] [M] | [$CO_2$] [M] | $k_{obs}$ [$s^{-1}$] | $k_2$ [$M^{-1}$ $s^{-1}$] | [**1a**] [M] | [$CS_2$] [M] | $k_{obs}$ [$s^{-1}$] | $k_2$ [$M^{-1}$ $s^{-1}$] |
| $2.93 \times 10^{-5}$ | $18.1 \times 10^{-3}$ | $3.78 \times 10^{-5}$ | $(2.11 \pm 0.08) \times 10^{-3}$ | $5.23 \times 10^{-5}$ | $2.92 \times 10^{-3}$ | $2.95 \times 10^{-2}$ | $10.2 \pm 0.3$ |
| $2.98 \times 10^{-5}$ | $13.6 \times 10^{-3}$ | $2.96 \times 10^{-5}$ | | $5.23 \times 10^{-5}$ | $1.95 \times 10^{-3}$ | $2.08 \times 10^{-2}$ | |
| $3.02 \times 10^{-5}$ | $9.06 \times 10^{-3}$ | $2.11 \times 10^{-5}$ | | $5.23 \times 10^{-5}$ | $9.74 \times 10^{-4}$ | $1.04 \times 10^{-2}$ | |
| $3.07 \times 10^{-5}$ | $4.75 \times 10^{-3}$ | $1.59 \times 10^{-5}$ | | | | | |

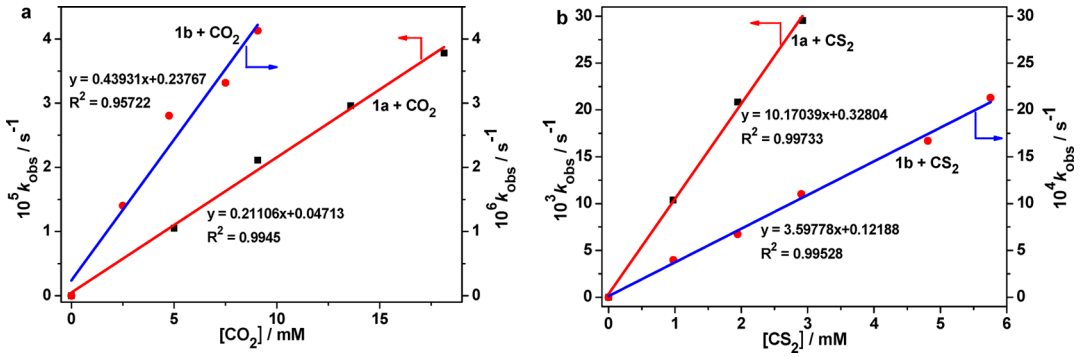


**Figure 5.** Relationship between the observed pseudo-first-order rate constants ($k_{obs}$) of $CX_2$ (X = O, S) insertion into ruthenium hydrides and the concentration of $CX_2$ (X = O, S) in $CH_3CN$ solution under 1 atm of Ar at 25 °C.

**Table 6. Second-Order Rate Constants ($k_2$) for the Reaction of 1a and 1b with $CO_2$ and $CS_2$ in Various Solvents under 1 atm of Ar at 25 °C Obtained from UV−Vis Spectra for the Kinetic Measurements under the Selected Wavelengths ($\lambda$)**

| | | | **1a** + $CO_2$ | | **1b** + $CO_2$ | | **1a** + $CS_2$ | | **1b** + $CS_2$ | |
|---|---|---|---|---|---|---|---|---|---|---|
| solvent | AN[a] | $D_s$[b] | $k_2$ [$M^{-1}$ $s^{-1}$] | $\lambda$ [nm] | $k_2$ [$M^{-1}$ $s^{-1}$] | $\lambda$ [nm] | $k_2$ [$M^{-1}$ $s^{-1}$] | $\lambda$ [nm] | $k_2$ [$M^{-1}$ $s^{-1}$] | $\lambda$ [nm] |
| MeOH | 41.3 | 32.6 | $(1.13 \pm 0.08) \times 10^{-1}$ | 514 | $(1.46 \pm 0.09) \times 10^{-3}$ | 510 | $3.43 \pm 0.10$ | 420 | $0.27 \pm 0.01$ | 418 |
| $CH_3CN$ | 18.9 | 36.1 | $(2.11 \pm 0.08) \times 10^{-3}$ | 528 | $(4.39 \pm 0.46) \times 10^{-4}$ | 510 | $10.2 \pm 0.3$ | 425 | $0.36 \pm 0.06$ | 418 |
| DMF | 16.0 | 36.7 | $(3.22 \pm 0.14) \times 10^{-3}$ | 534 | $(6.58 \pm 0.07) \times 10^{-4}$ | 522 | $24.0 \pm 0.5$ | 428 | $1.02 \pm 0.02$ | 421 |
| acetone | 12.5 | 20.7 | $(9.40 \pm 0.41) \times 10^{-4}$ | 532 | $(4.11 \pm 0.17) \times 10^{-4}$ | 510 | $8.51 \pm 0.22$ | 528 | $0.25 \pm 0.01$ | 508 |

[a]AN indicates the acceptor number of the solvent.[12,17,62] [b]$D_s$ donates the static dielectric constant of solvent.[17,63,64]

described in Table 5, according to the pseudo-first-order equation. Figure 5a illustrates the plots of $k_{obs}$ for $CO_2$ insertion into a ruthenium hydride complex versus the concentration of $CO_2$ in acetonitrile solution; the linear relationship between the $k_{obs}$ and the $CO_2$ concentration thus supported the hypothesis of the second-order reaction for a ruthenium hydride complex and $CO_2$. Table 5 shows the initial concentrations of **1a** and $CO_2$ in $CH_3CN$ under 1 atm of Ar at 25 °C for Figure 4; from a linear plot of $k_{obs}$ versus $CO_2$ concentration (Figure 4a), the second-order rate constant ($k_2$) of the reaction was determined as $(2.11 \pm 0.08) \times 10^{-3}$ $M^{-1}$ $s^{-1}$ in $CH_3CN$ at 25 °C.

To probe the correlation between rate constant and solvent property, the acceptor number (AN) of solvent was subjected to the $CO_2$ insertion reaction. AN was deduced from $^{31}P$ NMR studies on triethylphosphine oxide in different solvents by Gutmann and reflects the electrophilic properties of the


dx.doi.org/10.1021/ic500866d | Inorg. Chem. 2014, 53, 9570−9580

solvent.[62,12] Creutz and Ishitani suggested that the negative charge on the hydride ligand in a metal hydride complex can be increasingly stabilized with the increasing AN of solvent.[12,17] In our case, as shown in Table 6, the second-order rate constant for the reaction of **1a** and $CO_2$ increases with the AN of solvents from $(9.40 \pm 0.41) \times 10^{-4}$ $M^{-1}$ $s^{-1}$ in acetone (AN = 12.5) to $(1.13 \pm 0.08) \times 10^{-1}$ $M^{-1}$ $s^{-1}$ in methanol (AN = 41.3). Notably, the reaction rate of **1a** and $CO_2$ in methanol is about 3 orders of magnitude faster than in acetone (Table 6). In principle, our reported results seemed to agree with the mechanism proposed by Creutz and Ishitani, indicating that the solvent with the highest AN proved to be most active to promote the $CO_2$ insertion into the **1a**. In addition, both water (AN = 55) and methanol (AN = 41.3) show higher AN values among the investigated solvents. Therefore, our reported kinetics results further support the experimental observation that the addition of water or methanol enhanced the $CO_2$ hydrogenation with the transition metal complexes as catalysts.[30−33] In the case of **1b**, the second-order rate constant of $CO_2$ insertion into the Ru−H bond of **1b** ranges from $(4.11 \pm 0.17) \times 10^{-4}$ $M^{-1}$ $s^{-1}$ in acetone to $(1.46 \pm 0.09) \times 10^{-3}$ $M^{-1}$ $s^{-1}$ in methanol, which is much slower than that of **1a**. Similarly, the second-order rate constants for the reaction of **1b** and $CO_2$ increase with the AN of solvents (Table 6). In addition, Figure 6 further provides a deeper insight into the

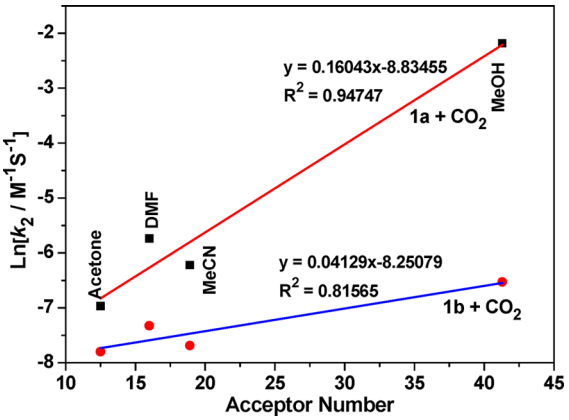


**Figure 6.** Relationship between the second-order rate constants ($k_2$) of $CO_2$ insertion measured in various solvents and the acceptor numbers (AN) of the solvents.

relationship between the reactivity of a ruthenium hydride complex toward $CO_2$ and the nature of solvent, showing a linear correspondence between the Ln($k_2$) and the AN of the solvents for the reactions of **1a** or **1b** and $CO_2$.

In addition to $CO_2$, the kinetics of $CS_2$ insertion into the ruthenium hydride complexes were performed with a similar procedure to that of $CO_2$ (Figures 1c, 4b, and 5b). In contrast, the second-order rate constant of $CS_2$ insertion into **1a** varied from $(3.43 \pm 0.10)$ $M^{-1}$ $s^{-1}$ in methanol to $(24.0 \pm 0.5)$ $M^{-1}$ $s^{-1}$ in DMF (Table 6), which is almost 4 orders of magnitude faster than in the case of $CO_2$ insertion. The results described in Table 6 thus quantitatively reveal a higher reactivity of $CS_2$ toward **1a** than that of $CO_2$. In the case of **1b**, the reaction rate of **1b** with $CS_2$ was many times slower than that of **1a**; moreover, the reaction rate of **1b** with $CS_2$ is 3 orders of magnitude faster than that of $CO_2$ under the investigated conditions (Table 6). However, the expected correlation between the Ln($k_2$) of $CS_2$ insertion into the ruthenium hydride complex (**1a** or **1b**) and the AN of the solvent was unobserved. In fact, the $k_2$ of $CS_2$ insertion into the ruthenium hydride complex (**1a** or **1b**) generally increased with the static dielectric constant ($D_s$) of the solvent used (Table 6).

The influence of a solvent on a hydride ligand revealed that the AN of solvent shows the ability of a solvent to accept electron density and relates with the Lewis acidity of the solvent. Therefore, the stabilization effect of solvent toward a hydride ligand increases with the AN of solvent. Our reported results thus suggested that the activation of a hydride ligand in the complex toward $CO_2$ fixation reaction is governed by the AN of the solvent, showing that the stronger the Lewis acidity of the solvent is, the faster the reaction goes.[15] The comparison of $CO_2$ and $CS_2$ molecules shows that both $CO_2$ and $CS_2$ are linear triatomic molecules. However, according to the literature, the ionization potentials of $CS_2$ and $CO_2$ are 10.09 and 13.78 eV, respectively.[45] Moreover, the electron affinities of $CS_2$ and $CO_2$ are 1.0 and −0.6 eV, respectively. Therefore, $CS_2$ is a better $\sigma$-donor and a better $\pi$-acceptor than $CO_2$. Moreover, $CS_2$ is a very reactive molecule toward transition metal complexes than $CO_2$ although $CS_2$ and $CO_2$ are structurally similar. The fact that the reaction rate of $CS_2$ insertion is faster than $CO_2$ can be attributed to the higher reactivity of $CS_2$. However, the reactivity of $CS_2$ with ruthenium hydride complexes in various solvents was not governed by the AN of solvents used. In fact, the mild Lewis-base solvent can promote the reaction. As the $D_s$ of a solvent reflects its chemical polarity,[64] the fact that the $k_2$ of $CS_2$ insertion into ruthenium hydride generally increases with $D_s$ of the reaction medium suggests that the interactions between the solvent and $CS_2$ induce electric dipole moment of $CS_2$ molecule, increase the polarizability of $CS_2$ in the reaction medium, and promote the nucleophilic attack of the hydride ligand to the carbon atom of $CS_2$.[33]

It was suggested that the nucleophilic attack of the hydride ligand to the carbon atom of $CO_2$ is the rate-determining step during the $CO_2$ insertion into ruthenium hydride.[12,17,25] In principle, our results are consistent with the references. The Lewis acid center of solvent molecules polarizes $CO_2$ molecule by interacting with the oxygen atom of $CO_2$; accordingly, the carbon atom is more liable to be nucleophilically attacked by a hydride ligand from the hydrido complex.[17] At the same time, Lewis-acid solvent would decrease the electron density of the hydride ligand and weaken its activities.[12] Therefore, the influence of Lewis-acid solvent toward $CO_2$ is the key factor during the insertion reaction, owing to the inert properties of $CO_2$.[12,13] It is well-known that AN is closely relate with the Lewis acidity of solvent,[12,17,60] the influence of solvent can thus cause approximately 3 orders of magnitude difference in the second order rate constant when the AN of solvents ranged from 12.5 to 41.3 (Table 6).

The mechanism of the $CS_2$ insertion reaction includes the nucleophilic attack of the hydride ligand to the carbon atom of $CS_2$ and the interaction of transition metal center with sulfur terminus of $CS_2$ in the transition state.[23,30,33,54] However, the second order rate constant was gently governed by the $D_s$ of the the solvent. This result may be attributed to the higher reactivity of $CS_2$;[45,46] therefore, the influence of solvent polarity toward $CS_2$ molecule plays a minor role when the insertion happens. Nevertheless, this influence can only cause approximately an order of magnitude difference in rate constants, owing to the higher reactivity of $CS_2$ (Table 6).


dx.doi.org/10.1021/ic500866d | Inorg. Chem. 2014, 53, 9570−9580

## CONCLUSIONS

In summary, we report the structural, spectroscopic, and electrochemical properties of the ruthenium hydride complexes of $[Ru(H)(bpy)_2(PTA)]PF_6$ (**1a**) and $[Ru(H)(bpy)_2(PPh_3)]PF_6$ (**1b**). Both two hydride complexes quantitatively react with $CO_2$ and $CS_2$ to give the corresponding formate complexes $[Ru(\eta^1\text{-}OC(H)=O)(bpy)_2(L)]PF_6$ (L = PTA for **2a**, and $PPh_3$ for **2b**) and dithioformate complexes $[Ru(\eta^1\text{-}SC(H)=S)(bpy)_2(L)]PF_6$ (L = PTA for **3a**, and $PPh_3$ for **3b**), respectively. Both the insertions of $CO_2$ and $CS_2$ into **1a** follow second-order kinetics. The second-order rate constant ($k_2$) of $CO_2$ insertion into **1a** varied from $(9.40 \pm 0.41) \times 10^{-4}$ $M^{-1}$ $s^{-1}$ in acetone to $(1.13 \pm 0.08) \times 10^{-1}$ $M^{-1}$ $s^{-1}$ in methanol, whereas the $k_2$ of the $CS_2$ insertion reaction ranged from $(3.43 \pm 0.10)$ $M^{-1}$ $s^{-1}$ in methanol to $(24.0 \pm 0.5)$ $M^{-1}$ $s^{-1}$ in DMF. The reactivity of **1b** with $CO_2$ and $CS_2$ is slower than that of **1a** under the investigated conditions. The relationship between the $k_2$ of $CO_2$ insertion into ruthenium hydrides and the acceptor number (AN) of the solvents shows a linear correspondence between $Ln(k_2)$ and AN. Although, the $k_2$ of $CS_2$ insertion generally increased with static dielectric constant ($D_s$) of the reaction medium investigated. The structures of **1a**, **1b**, and **2b** were determined by X-ray crystallographic analysis.

## ASSOCIATED CONTENT

### Supporting Information

$^1H$ NMR, $^{31}P$ NMR, and FT-IR spectra of **1a**−**4b**. This material is available free of charge via the Internet at http://pubs.acs.org. Further atomic parameters, bond lengths, bond angles and thermal parameters have been deposited at the Cambridge Crystallographic Data Centre, CCDC No. 995663 for **1a**, No. 995662 for **1b**, and No. 995664 for **2b**, respectively.

## AUTHOR INFORMATION

### Corresponding Author

*Tel./Fax: (+86)20-3722-3380. E-mail: chenjz@ms.giec.ac.cn.

### Notes

The authors declare no competing financial interest.

## ACKNOWLEDGMENTS

We are grateful for the financial support from National Natural Science Foundation of China (21172219, 21207039, and 21303209), 100 Talents Program of the Chinese Academy of Sciences, and Guangdong Provincial Key Laboratory of Atmospheric Environment and Pollution Control.

## REFERENCES

(1) Morris, A. J.; Meyer, G. J.; Fujita, E. *Acc. Chem. Res.* **2009**, *42*, 1983−1994.
(2) Bensaid, S.; Centi, G.; Garrone, E.; Perathoner, S.; Saracco, G. *ChemSusChem* **2012**, *5*, 500−521.
(3) Benson, E. E.; Kubiak, C. P.; Sathrum, A. J.; Smieja, J. M. *Chem. Soc. Rev.* **2009**, *38*, 89−99.
(4) Gattrell, M.; Gupta, N.; Co, A. *J. Electroanal. Chem.* **2006**, *594*, 1−19.
(5) Wang, W.; Wang, S. P.; Ma, X. B.; Gong, J. L. *Chem. Soc. Rev.* **2011**, *40*, 3703−3727.
(6) Jessop, P. G.; Joó, F.; Tai, C. C. *Coord. Chem. Rev.* **2004**, *248*, 2425−2442.
(7) Jessop, P. G.; Ikariya, T.; Noyori, R. *Chem. Rev.* **1995**, *95*, 259−272.
(8) Leitner, W. *Angew. Chem., Int. Ed. Engl.* **1995**, *34*, 2207−2221.
(9) Nagao, H.; Mizukawa, T.; Tanaka, K. *Inorg. Chem.* **1994**, *33*, 3415−3420.
(10) Kim, S. S.; Lee, H. H.; Hong, S. C. *Appl. Catal. A Gen.* **2012**, *423*, 100−107.
(11) Creutz, C.; Chou, M. H. *J. Am. Chem. Soc.* **2009**, *131*, 2794−2795.
(12) Creutz, C.; Chou, M. H. *J. Am. Chem. Soc.* **2007**, *129*, 10108−10109.
(13) Creutz, C.; Chou, M. H.; Hou, H.; Muckerman, J. T. *Inorg. Chem.* **2010**, *49*, 9809−9822.
(14) Chen, J. Z.; Szalda, D. J.; Fujita, E.; Creutz, C. *Inorg. Chem.* **2010**, *49*, 9380−9391.
(15) Kern, S.; van Eldik, R. *Inorg. Chem.* **2012**, *51*, 7340−7345.
(16) Hayashi, H.; Ogo, S.; Abura, T.; Fukuzumi, S. *J. Am. Chem. Soc.* **2003**, *125*, 14266−14267.
(17) Konno, H.; Kobayashi, A.; Sakamoto, K.; Fagalde, F.; Katz, N. E.; Saitoh, H.; Ishitani, O. *Inorg. Chim. Acta* **2000**, *299*, 155−163.
(18) Albertin, G.; Antoniutti, S.; Bacchi, A.; D'Este, C.; Pelizzi, G. *Inorg. Chem.* **2004**, *43*, 1336−1349.
(19) Chakraborty, S.; Zhang, J.; Krause, J. A.; Guan, H. R. *J. Am. Chem. Soc.* **2010**, *132*, 8872−8873.
(20) Schmeier, T. J.; Hazari, N.; Incarvito, C. D.; Raskatov, J. A. *Chem. Commun.* **2011**, *47*, 1824−1826.
(21) Yoo, C.; Kim, J.; Lee, Y. *Organometallics* **2013**, *32*, 7195−7203.
(22) Venkanna, G. T.; Tammineni, S.; Arman, H. D.; Tonzetich, Z. J. *Organometallics* **2013**, *32*, 4656−4663.
(23) Field, L. D.; Lawrenz, E. T.; Shaw, W. J.; Turner, P. *Inorg. Chem.* **2000**, *39*, 5632−5638.
(24) Hayashi, H.; Ogo, S.; Fukuzumi, S. *Chem. Commun.* **2004**, 2714−2715.
(25) Ogo, S.; Kabe, R.; Hayashi, H.; Harada, R.; Fukuzumi, S. *Dalton Trans.* **2006**, 4657−4663.
(26) Ng, S. M.; Yin, C. Q.; Yeung, C. H.; Chan, T. C.; Lau, C. P. *Eur. J. Inorg. Chem.* **2004**, 1788−1793.
(27) Tanaka, R.; Yamashita, M.; Nozaki, K. *J. Am. Chem. Soc.* **2009**, *131*, 14168−14169.
(28) Tsai, J.-C.; Nicholas, K. M. *J. Am. Chem. Soc.* **1992**, *114*, 5117−5124.
(29) Tai, C.-C.; Pitts, J.; Linehan, J. C.; Main, A. D.; Munshi, P.; Jessop, P. G. *Inorg. Chem.* **2002**, *41*, 1606−1614.
(30) Chu, H. S.; Lau, C. P.; Wong, K. Y. *Organometallics* **1998**, *17*, 2768−2777.
(31) Munshi, P.; Main, A. D.; Linehan, J. C.; Tai, C.-C.; Jessop, P. G. *J. Am. Chem. Soc.* **2002**, *124*, 7963−7971.
(32) Yin, C. Q.; Xu, Z. T.; Yang, S. Y.; Ng, S. M.; Wong, K. Y.; Lin, Z. Y.; Lau, C. P. *Organometallics* **2001**, *20*, 1216−1222.
(33) Matsubara, T.; Hirao, K. *Organometallics* **2001**, *20*, 5759−5768.
(34) Muckerman, J. T.; Achord, P.; Creutz, C.; Polyansky, D. E.; Fujita, E. *Proc. Natl. Acad. Sci. U. S. A.* **2012**, *109*, 15657−15662.
(35) Matsubara, T. *Organometallics* **2001**, *20*, 19−24.
(36) Ohnishi, Y. Y.; Matsunaga, T.; Nakao, Y.; Sato, H.; Sakaki, S. *J. Am. Chem. Soc.* **2005**, *127*, 4021−4032.
(37) Kovács, G.; Schubert, G.; Joó, F.; Pápai, I. *Catal. Today* **2006**, *115*, 53−60.
(38) Ohnishi, Y. Y.; Nakao, Y.; Sato, H.; Sakaki, S. *Organometallics* **2006**, *25*, 3352−3363.
(39) Urakawa, A.; Jutz, F.; Laurenczy, G.; Baiker, A. *Chem.—Eur. J.* **2007**, *13*, 3886−3899.
(40) Musashi, Y.; Sakaki, S. *J. Am. Chem. Soc.* **2002**, *124*, 7588−7603.
(41) Hutschka, F.; Dedieu, A.; Leitner, W. *Angew. Chem., Int. Ed. Engl.* **1995**, *34*, 1742−1745.
(42) Hutschka, F.; Dedieu, A.; Eichberger, M.; Fornika, R.; Leitner, W. *J. Am. Chem. Soc.* **1997**, *119*, 4432−4443.
(43) Matsubara, Y.; Fujita, E.; Doherty, M. D.; Muckerman, J. T.; Creutz, C. *J. Am. Chem. Soc.* **2012**, *134*, 15743−15757.
(44) Matsubara, Y.; Hightower, S. E.; Chen, J. Z.; Grills, D. C.; Polyansky, D. E.; Muckerman, J. T.; Tanaka, K.; Fujita, E. *Chem. Commun.* **2014**, *50*, 728−730.
(45) Pandey, K. K. *Coord. Chem. Rev.* **1995**, *140*, 37−114.

(46) Ibers, J. A. *Chem. Soc. Rev.* **1982**, *11*, 57−73.
(47) Anderson, J. S.; Iluc, V. M.; Hillhouse, G. L. *Inorg. Chem.* **2010**, *49*, 10203−10207.
(48) Haack, P.; Limberg, C.; Tietz, T.; Metzinger, R. *Chem. Commun.* **2011**, *47*, 6374−6376.
(49) Matson, E. M.; Forrest, W. P.; Fanwick, P. E.; Bart, S. C. *J. Am. Chem. Soc.* **2011**, *133*, 4948−4954.
(50) Bheemaraju, A.; Beattie, J. W.; Lord, R. L.; Martin, P. D.; Groysman, S. *Chem. Commun.* **2012**, *48*, 9595−9597.
(51) Bianchini, C.; Ghilardi, C. A.; Meli, A.; Midollini, S.; Orlandini, A. *Inorg. Chem.* **1985**, *24*, 932−939.
(52) Albertin, G.; Antoniutti, S.; Delministro, E.; Bordignon, E. *Dalton Trans.* **1994**, 1769−1775.
(53) Lindner, E.; Lin, Y. C.; Geprägs, M.; Yih, K. H.; Fawzi, R.; Steimann, M. *J. Organomet. Chem.* **1996**, *512*, 101−110.
(54) Gandhi, T.; Nethaji, M.; Jagirdar, B. R. *Inorg. Chem.* **2003**, *42*, 4798−4800.
(55) Nanishankar, H. V.; Dutta, S.; Nethaji, M.; Jagirdar, B. R. *Inorg. Chem.* **2005**, *44*, 6203−6210.
(56) Albertin, G.; Antoniutti, S.; Roveda, G. *Inorg. Chim. Acta* **2005**, *358*, 3093−3105.
(57) Daigle, D. J. *Inorg. Synth.* **1998**, *32*, 40−45.
(58) Sullivan, B. P.; Salmon, D. J.; Meyer, T. J. *Inorg. Chem.* **1978**, *17*, 3334−3341.
(59) Fujita, E.; Szalda, D. J.; Creutz, C.; Sutin, N. *J. Am. Chem. Soc.* **1988**, *110*, 4870−4871.
(60) Schmidt, M. H.; Miskelly, G. M.; Lewis, N. S. *J. Am. Chem. Soc.* **1990**, *112*, 3420−3426.
(61) Kelly, J. M.; Vos, J. G. *Dalton Trans.* **1986**, 1045−1048.
(62) Gutmann, V. *Electrochim. Acta* **1976**, *21*, 661−670.
(63) Sullivan, B. P.; Meyer, T. J. *Organometallics* **1986**, *5*, 1500−1502.
(64) Weast, R. C.; Lide, D. R.; Astle, M. J.; Beyer, W. H. *CRC Handbook of Chemistry and Physics*, 70th ed.; CRC Press: Boca Raton, FL, 1990.